Journal of Electroanalytical Chemistry 952 (2024) 117997

Contents lists available at ScienceDirect

Journal of Electroanalytical Chemistry

journal homepage: www.elsevier.com/locate/jelechem

Ruthenium,nitrogen-codoped carbon aerogels for real-time electrochemical monitoring of cellular hydrogen peroxide release

Ruiling Qiao [a,1], Yongmin Lei [b,1], Qiming Liu [c], Lina Tang [a,e], Xueqian Xiao [a], Guojun Zhang [a,e], Ting He [d], Yulin Zhang [a,e,*], Chunzi Liang [a,e,*], Shaowei Chen [c,*]

[a] School of Laboratory Medicine, Hubei University of Chinese Medicine, Wuhan, Hubei 430065, China
[b] College of Information Engineering, Hubei University of Chinese Medicine, Wuhan, Hubei 430065, China
[c] Department of Chemistry and Biochemistry, University of California, 1156 High Street, Santa Cruz, CA 95064, USA
[d] School of Materials Science and Engineering, Xiangtan University, Xiangtan, Hunan 411105, China
[e] Hubei Shizhen Laboratory, Wuhan, Hubei 430065, China

ARTICLE INFO

Keywords:
Hydrogen peroxide
Ruthenium,nitrogen-codoped carbon aerogel
Electrochemical sensor
Living cell
Anticancer drug

ABSTRACT

Hydrogen peroxide (H_2O_2) is an important signaling molecule for diverse biological functions, and it is thus of importance to develop sensing platforms for real-time monitoring of cellular release of H_2O_2. Herein, a H_2O_2 electrochemical sensor is constructed based on ruthenium,nitrogen-codoped carbon aerogels. The nanocomposites are prepared by controlled pyrolysis of a biomass hydrogel with $RuCl_3$, where RuN_x single-atom sites and Ru nanoclusters are incorporated into the aerogel scaffold, as confirmed by high-angle annular dark-field scanning transmission electron microscopy and X-ray photoelectron spectroscopy measurements. In cyclic voltammetry and amperometric analysis, the aerogels exhibit a remarkable H_2O_2 detection performance, with excellent sensitivity and selectivity, wide linear range (0.1 μM ~ 1 mM) and low detection limit (0.01 μM). The sensor can also be used for real-time monitoring of hydrogen peroxide released from MCF-7 cells and screening of anticancer drugs, displaying a high potential for biosensing and biomedical diagnostics.

1. Introduction

Reactive oxygen species (ROS) are important cell signaling molecules and involved in the regulation of a number of biological processes in the body, including DNA damage, protein synthesis, and apoptosis [1]. Overabundance of ROS usually leads to excessive oxidative stress, and hence a variety of pathological reactions [2,3]. Consequently, the detection of intracellular ROS represents a critical first step towards a good understanding of the relationship between ROS concentration and clinical diseases and of the mechanism of their biological functions. Hydrogen peroxide (H_2O_2), an important ROS, has received much attention because of its significance in the growth, development and health of living organisms [4]. An imbalance in H_2O_2 production can lead to intracellular oxidative stress, and hence cellular damage and inhibition of cellular enzyme activity, affecting the growth and development of the organisms and promoting tumorigenesis [5,6]. Therefore, it is important to develop rapid and sensitive platforms for the accurate detection of H_2O_2 and to monitor its dynamic release process from living cells in order to assess the degree of oxidative stress in cells and the state of health of the organisms. In addition, as certain anticancer drugs can inhibit cancer cells by regulating the production of H_2O_2 and hence killing the tumor cells, a reliable H_2O_2 sensor can also be exploited for the screening and evaluation of the efficacy of anticancer drugs [7].

Many analytical techniques have been developed for H_2O_2 detection, such as colorimetric, titrimetric, chromatographic, spectrophotometric, and fluorescent methods [8,9]. However, these methods usually require sophisticated instrumentation, cumbersome operation and time-consuming procedure; and the low concentration and unstable character of H_2O_2 in the body makes its quantitative detection challenging [10,11]. Therefore, it is of fundamental significance to develop sensitive and rapid methods for the accurate monitoring of H_2O_2 concentration. Among these, electrochemical methods stand out due to its advantages of rapid response, easy operation, simple instrumentation and low cost [12]. However, the electrochemical performance may be compromised by the slow electron-transfer kinetics at the electrode surface, low sensitivity, and susceptibility to interference by other substances,

* Corresponding authors.
E-mail addresses: zhangyulin2001@163.com.cn (Y. Zhang), liangcz2021@hbtcm.edu.cn (C. Liang), shaowei@ucsc.edu (S. Chen).
[1] These authors contributed equally to this work.

https://doi.org/10.1016/j.jelechem.2023.117997
Received 20 October 2023; Received in revised form 30 November 2023; Accepted 14 December 2023
Available online 19 December 2023

leading to limited applications. This can be mitigated by deliberate engineering of the active materials loaded onto the electrode surface. For example, Singh et al. [13] modified an electrode surface with brominated graphene (GBR), a metal-free reduced graphene analog that mimicked peroxidase in the electrocatalytic decomposition of H_2O_2, where the electron transfer between the labile bromine/oxygen moieties in GBR and H_2O_2 facilitated the formation of peroxyhydroxyl radicals (HO_2·), leading to complete electro-oxidation of H_2O_2 at pH 7.2. In another study, Atacan et al. [14] constructed an electrochemical H_2O_2 sensor based on a glassy carbon electrode (GCE) modified with cupric oxide/graphitic carbon nitride (CuO/g-C_3N_4) composites (CuO is a redox-active and chemically robust p-type semiconductor with a band gap of ca. 1.5 eV and a high isoelectric point) [15], due to enhanced electrical conductivity and reduced agglomeration of CuO during the electrochemical reaction. The resulting sensor showed a linear response to H_2O_2 in the range of 0.5 to 50 μM, with a detection limit of 0.31 μM. In these studies, the chemically modified electrodes exhibit markedly improved sensitivity, as compared to the bare counterparts. Yet, most of the electrodes need to operate at a negative potential for H_2O_2 electrocatalysis, which may compromise the internal environment of the organism and generate responses to non-specific interactions. Hence, further improvement of the detection sensitivity and selectivity is desired [16,17].

Towards this end, noble metal nanoparticles have received extensive attention due to their unique catalytic activity towards H_2O_2 decomposition [18]. For example, Hu et al. [19] prepared platinum nanoparticles (Pt NPs) by using tea polyphenol (Tp) as a reducing agent. The obtained Tp-R-Pt modified electrode showed a satisfactory performance towards H_2O_2 sensing, as Pt NPs facilitated the adsorption and decomposition of H_2O_2. Peña et al. [20] prepared composites based on ruthenium oxide hexacyanoferrate (RuOHCF) and multi-walled carbon nanotubes (MWCNTs), and used the composites to construct a sensor for real-time monitoring of H_2O_2 during Fenton reaction, where the Ru(II/III) centers catalyzed the reduction of H_2O_2. One may notice that these sensing platforms are based on precious metals [21]. To reduce the materials costs, single-atom catalysts (SACs) have emerged as a unique option [22,23]. For instance, Xie et al. [24] prepared a Ru SAC-based enzyme mimic (Ru-Ala-C_3N_4) by atomically dispersing Ru centers into a g-C_3N_4 scaffold, where the Ru—N—C coordination moieties served as the catalytic active centers, markedly boosted the charge-transfer kinetics, and enhanced the performance of H_2O_2 detection. In these SACs, the electrochemical performance is closely correlated to the coordination configurations of the single atom moieties [25–27]. Carbon aerogels, with a 3D porous network structure, possess ultra-high porosity (80 %-99 %) for maximal metal loading and is an attractive structural scaffold [28,29]. Doping with select heteroatoms (e.g., N, P, S) is an effective strategy to immobilize the metal centers and minimize aggregation [30], where the ensuing metal–ligand interactions can be exploited for the manipulation of the charge density of the metal centers and electrical conductivity of the nanocomposites, leading to optimal catalytic activity [31].

In this study, ruthenium,nitrogen-codoped carbon aerogels (Ru-NCAG) were synthesized by high-temperature pyrolysis of a biomass hydrogel mixed with $RuCl_3$ [32], where RuN_x single atom moieties and Ru nanoclusters were embedded within the *N*-doped carbon scaffold at a high loading, due to spatial confinement of micropores and nanowrinkles of the aerogels. The obtained Ru-NCAG exhibited a remarkable catalytic activity and stability for H_2O_2 detection, with high selectivity even in the presence of excessive interfering substances. Notably, the Ru-NCAG-based electrochemical sensor could be used for real-time monitoring of H_2O_2 release in MCF-7 cells and for detection of H_2O_2 concentration after doxorubicin (DOX) drug stimulation of living cells, demonstrating unique potential for the clinical screening of antitumor drugs.

2. Experimental section

2.1. Materials and chemicals

Hydrogen peroxide (H_2O_2, 30 %) was purchased from Sinopharm Chemical Reagents Co. Ltd. (Shanghai, China). Glucose and phosphate buffered saline (PBS) were purchased from Generay Biotech Co. Ltd. (Shanghai, China). Ascorbic acid (AA), urea (Urea), uric acid (UA), dopamine hydrochloride (DA), *N*-formyl-Methionyl-leucyl-phenylalanine (fMLP), DOX and catalase were purchased from Sigma Aldrich (USA). Gelatin, potassium hydroxide (KOH), ruthenium(III) chloride ($RuCl_3$), zinc(II) acetate dihydrate ($Zn(Ac)_2{\cdot}2H_2O$) and SiO_2 nanoparticles were purchased at Aladdin Reagents (Shanghai, China). 1,10-Phenanthroline monohydrate, 5 % Nafion solution and RuO_2 were purchased from Sigma Aldrich. The cell culture medium DMEM was purchased from Procell Life Science & Technology Co. Ltd. (Wuhan, China). Cell Counting Kit-8 (CCK-8) was purchased from Meilun Biotechnology Co. Ltd. (Dalian, China). Human breast cancer cell MCF-7 was supplied by American Type Culture Collection (ATCC, Manassas, VA, USA). Ultrapure water was obtained from a Millipore water purification system (resistivity 18.2 MΩ cm, MilliQ Direct 8). All chemicals used in this study were of analytical grade and used without further purification.

2.2. Synthesis of Ru-NCAG

Ru-NCAG was synthesized by adopting a procedure described previously [32–34], as illustrated in Scheme 1a. In brief, 240 mg of gelatin, 200 mg of SiO_2 and 10 mL of MilliQ water were added to a vial under magnetic stirring in a 60 °C water bath for 10 min, into which were then added 400 μL of 0.05 M $RuCl_3$, 35.6 mg of 1,10-diazaphenanthrene and 320 μL of 1.0 M zinc acetate. The samples were then frozen at −20 °C for 8 h and thawed at 25 °C for 4 h. After three freezing-thawing cycles, a hydrogel was produced and pyrolyzed in a tube furnace with a constant flow rate of 97 % Ar + 3 % H_2 at 900 °C for 3 h. The obtained sample was cooled naturally at room temperature, and then etched with 3 wt% HF to remove the SiO_2 nanoparticles, affording Ru-NCAG. NCAG without Ru was prepared in the same manner, except that no $RuCl_3$ was added.

2.3. Structural characterization

Sample morphologies and atomic dispersion of Ru centers were examined with a transmission electron microscope (TEM, FEI Talos F200S) and high-angle annular dark-field scanning TEM (HAADF-STEM). X-ray photoelectron spectroscopy (XPS) measurements were carried out with an ESCALAB 250Xi instrument.

2.4. Electrode preparation and electrochemical study

The electrode preparation was schematically illustrated in Scheme 1b. Experimentally, a GCE (diameter 3 mm) was first polished to a mirror surface with 0.3 and 0.05 μm alumina powders, and then sonicated in pure water and ethanol for 3 min sequentially for three times to remove residues on the electrode surface. The electrode was then dried in a nitrogen stream. To prepare the catalyst ink, the Ru-NCAG synthesized above (1 mg) was added into a mixture of water, ethanol (v:v = 1:1, 950 μL in total) and Nafion solution (5 %, 50 μL) under sonication for 30 s to make a black suspension. 8 μL of the ink was dropcast onto the GCE surface and dried overnight at room temperature. All electrochemical tests were performed with a CHI 660E electrochemical workstation (CH Instruments, Shanghai, China), using the GCE as the working electrode, a saturated calomel electrode (SCE) as the reference electrode and a platinum wire as the counter electrode.

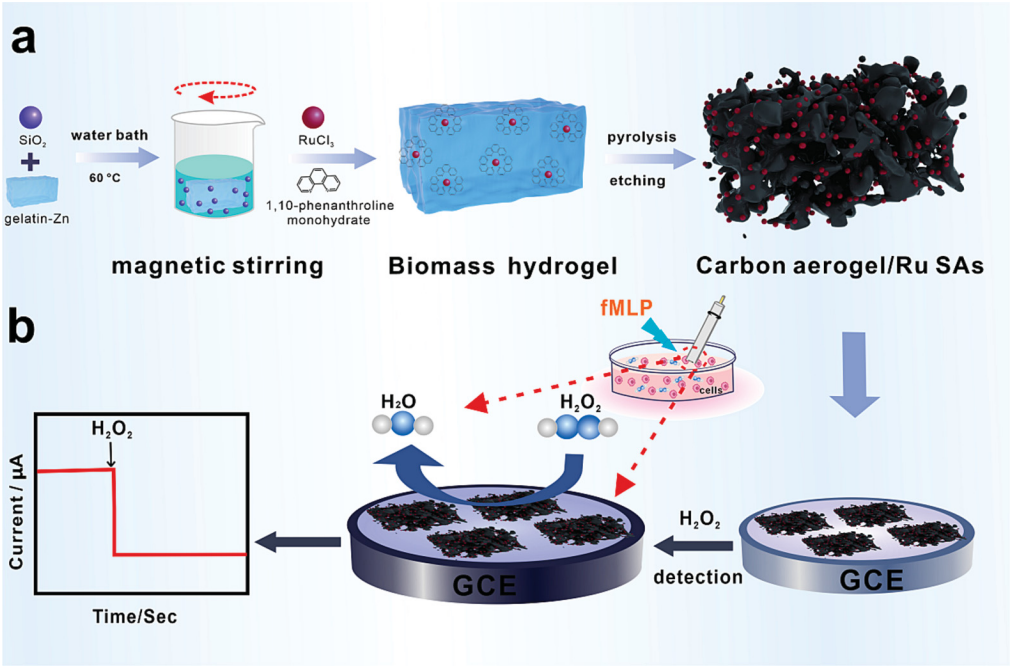

Scheme 1. Schematic illustrations of (a) the synthetic process of Ru-NCAG and (b) the detection of hydrogen peroxide released from living cells.

2.5. Cell culture and electrochemical detection of H_2O_2 release from MCF-7 cells

MCF-7 cells, which belong to the human breast cancer cell line, were selected as experimental cells in this study. The frozen MCF-7 cells were resuscitated and cultured in fresh complete medium (DEME) containing 10 % fetal bovine serum, 1 % penicillin and streptomycin under the environmental conditions of 37 °C, 95 % humidity and 5 % CO_2 [35]. A cell counter was used to estimate the cell number after it reached 90 % wall growth. After the cell supernatant medium was discarded, the cells were washed three times with sterile PBS buffer. Then trypsin digestion was added, followed by the addition of a sterile PBS buffer to make a cell suspension for the actual sample assay. In the real-time assay, H_2O_2 release from MCF-7 cells was assayed using Ru-NCAG/GCE at 0 V. MCF-7 cells were stimulated to produce H_2O_2 by adding 10 μL fMLP (10 μM) or DOX to the PBS solution containing the cells. As controls, 10 μL of fMLP or DOX was added to a PBS solution without cells and to a PBS solution containing a combination of both MCF-7 cells and catalase (50 μL, 300 U mL^{-1}).

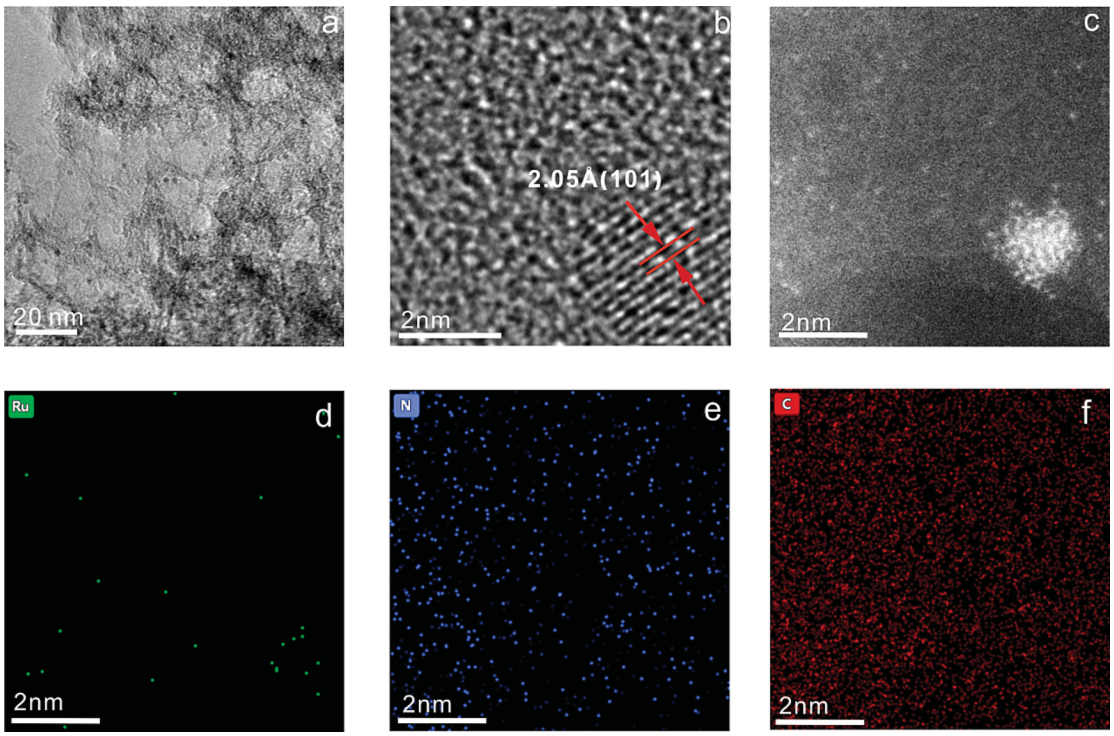

Fig. 1. (a) TEM image of Ru-NCAG. (b) HRTEM image of a metal nanocluster (scale bar 2 nm). (c) HAADF-STEM image and (d-f) elemental maps of Ru-NCAG.

3. Results and discussion

3.1. Structural characterization

From the TEM image in Fig. 1a, the Ru-NCAG sample can be seen to contain a small number of nanoclusters (ca. 2 nm in diameter) embedded within a carbon scaffold, which possessed well-defined lattice fringes with an interplanar d-spacing of 2.05 Å (Fig. 1b), in agreement with the (1 0 1) planes of *hcp* ruthenium [32]. Notably, in HAADF-STEM measurements a large number of single metal atoms can also be resolved within Ru-NCAG (Fig. 1c). This indicates that the Ru-NCAG sample contained a mixture of Ru single atoms and Ru nanoclusters. Elemental mapping analysis (Fig. 1d-f) showed that both N and Ru were uniformly dispersed within the carbon matrix without significant agglomeration, confirming the successful doping of these elements into the nanocomposites.

XPS measurements were then carried out to examine the chemical composition and elemental valence states of the materials. From the survey spectrum in Fig. 2a, the elements of C/Ru, N, and O can be readily identified in Ru-NCAG at ca. 285, 400 and 532 eV, respectively. Fig. 2b shows the high-resolution scan of the Ru 3p electrons, where two doublets can be deconvoluted at 463.68/485.78 and 461.78/484.38 eV, due to the $3p_{3/2}/3p_{1/2}$ electrons of metallic Ru and Ru(II), respectively [36,37]. This is consistent with the formation of ruthenium nanoclusters and atomically dispersed ruthenium in the carbon aerogels, which accounted for 12.8 % and 87.2 % of the total metal contents, respectively. Fig. 2c shows the corresponding N 1 s spectrum, where four N species were resolved, pyridinic N (398.33 eV), metal-N (398.87 eV), pyrrolic N (399.90 eV), graphitic N (400.78 eV) and oxidized N (401.26 eV). In the O 1 s spectrum (Fig. 2d), only two species were identified, C═O (532.08 eV) and C—O/O—H (533.48 eV), with no metal-O peak, suggesting the absence of metal oxides in the sample.

3.2. Electrochemical study

The electrochemical performance of Ru-NCAG was then tested by cyclic voltammetry (CV) and electrochemical impedance spectroscopy (EIS) measurements for H_2O_2 detection. Fig. 3a shows the CV curves of bare and Ru-NCAG modified GCE within the potential range of −0.2 to + 0.6 V in a 0.01 M PBS containing 5 mM $Fe[(CN)_6]^{3-/4-}$ at the scan rate of 100 mV s^{-1}. One can see that a pair of voltametric peaks can be resolved with a formal potential ($E^{o,}$) of + 0.117 V due to the Fe $[(CN)_6]^{3-/4-}$ redox chemistry; in addition, the double-layer charging current was markedly higher with the Ru-NCAG modified electrode than with the bare one, suggesting a significant increase of the specific surface area. The corresponding EIS profiles were collected at the open-circuit potential (Fig. 3b), where the bare electrode can be seen to exhibit an obvious semicircle in the high-frequency region, as compared to the Ru-NCAG modified one, suggesting a much reduced charge transfer resistance (R_{CT}) with the latter, which is conducive to H_2O_2 detection.

Fig. 3c shows the CV profiles in 5 mM $Fe[(CN)_6]^{3-/4-}$ at different scan rates (from 20 to 100 mV s^{-1}), where the cathodic and anodic peak currents can be seen to increase with increasing scan rates and showed a good linear relationship with the square root of potential scan rate (Fig. S1), suggesting a diffusion-controlled process. CV profiles were then collected with the bare, NCAG and Ru-NCAG modified GCE in a PBS solution in the absence and presence of H_2O_2. From Fig. 3d it can be seen that bare GCE and NCAG/GCE showed no significant voltametric currents with or without H_2O_2, whereas the Ru-NCAG modified electrode displayed an obvious reduction peak at + 0.146 V when H_2O_2 was added to the electrolyte solution, suggesting effective electrocatalytic activity of the Ru-NCAG composites towards H_2O_2 reduction, most likely due to the synergistic interactions between the Ru single atoms and nanoclusters [38,39]. Such a unique activity was then exploited for amperometric (i-t) detection of H_2O_2, where the initial potential was set at 0 V,

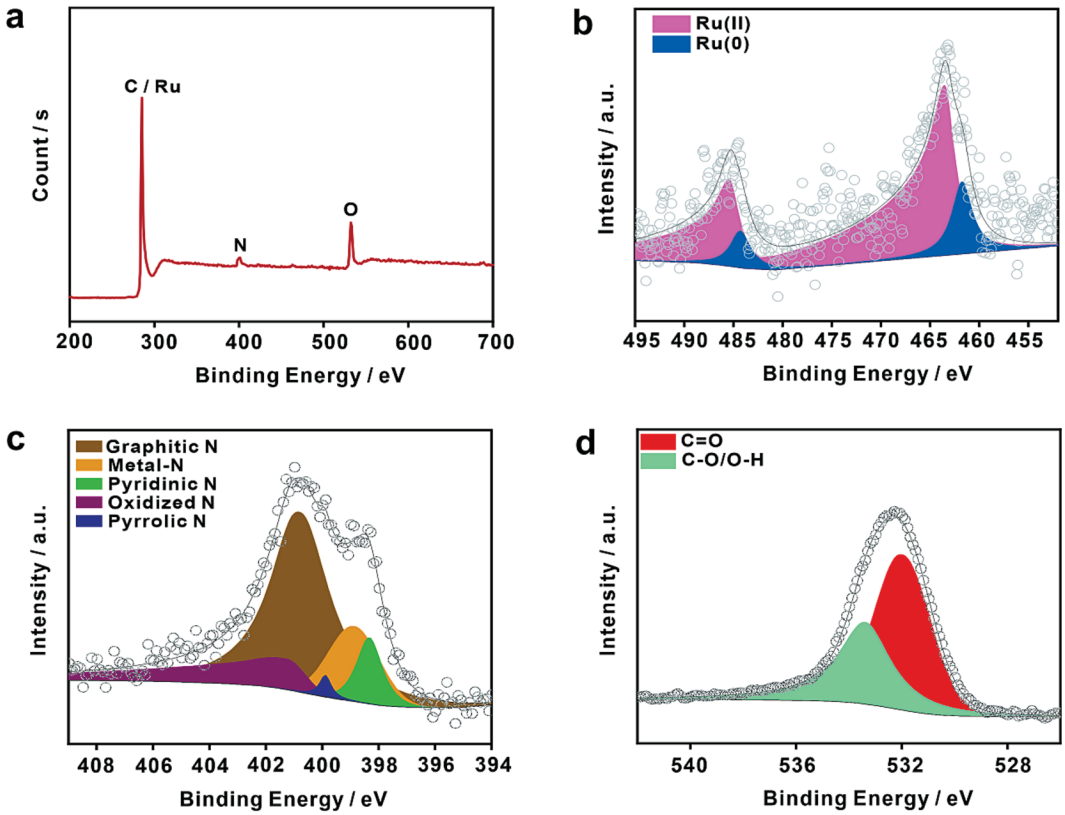

Fig. 2. (a) XPS survey spectrum and high-resolution scans of the (b) Ru 3p, (c) N 1 s and (d) O 1 s electrons of Ru-NCAG. In panel (b-d), symbols are experimental data and colored peaks are deconvolution fits.

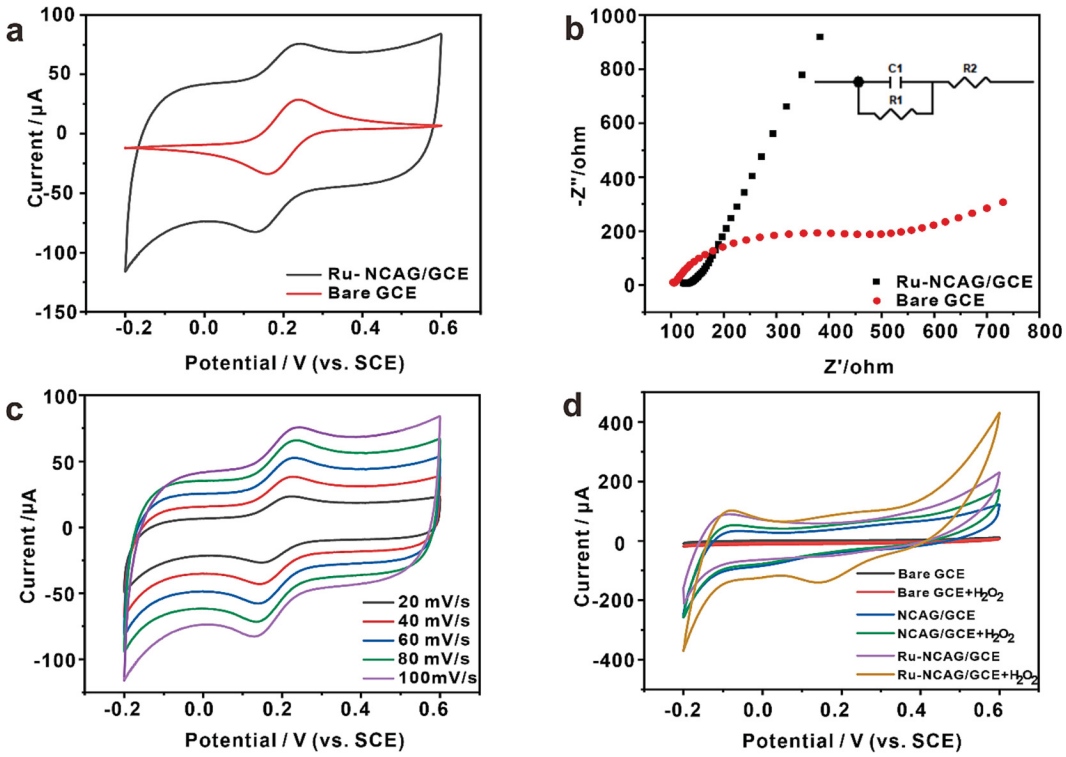

Fig. 3. (a) CV profiles of bare GCE and Ru-NCAG/GCE in a 0.01 M PBS containing 5 mM $[Fe(CN)_6]^{3-/4-}$ at a scan rate of 100 mV s^{-1}. (b) EIS profiles of bare GCE and Ru-NCAG/GCE in a 0.01 M PBS containing 5 mM $[Fe(CN)_6]^{3-/4-}$ at open circuit potential. Inset is the equivalent circuit, where R_1 is charge-transfer resistance, C_1 is double-layer capacitance, and R_2 is serial resistance. (c) CV profiles of Ru-NCAG/GCE in 0.01 M PBS containing 5 mM $[Fe(CN)_6]^{3-/4-}$ at different scanning rates. (d) CV profiles of NCAG/GCE, Ru-NCAG/GCE and bare GCE in a 0.01 M PBS solution in the absence and presence of 10 μM H_2O_2.

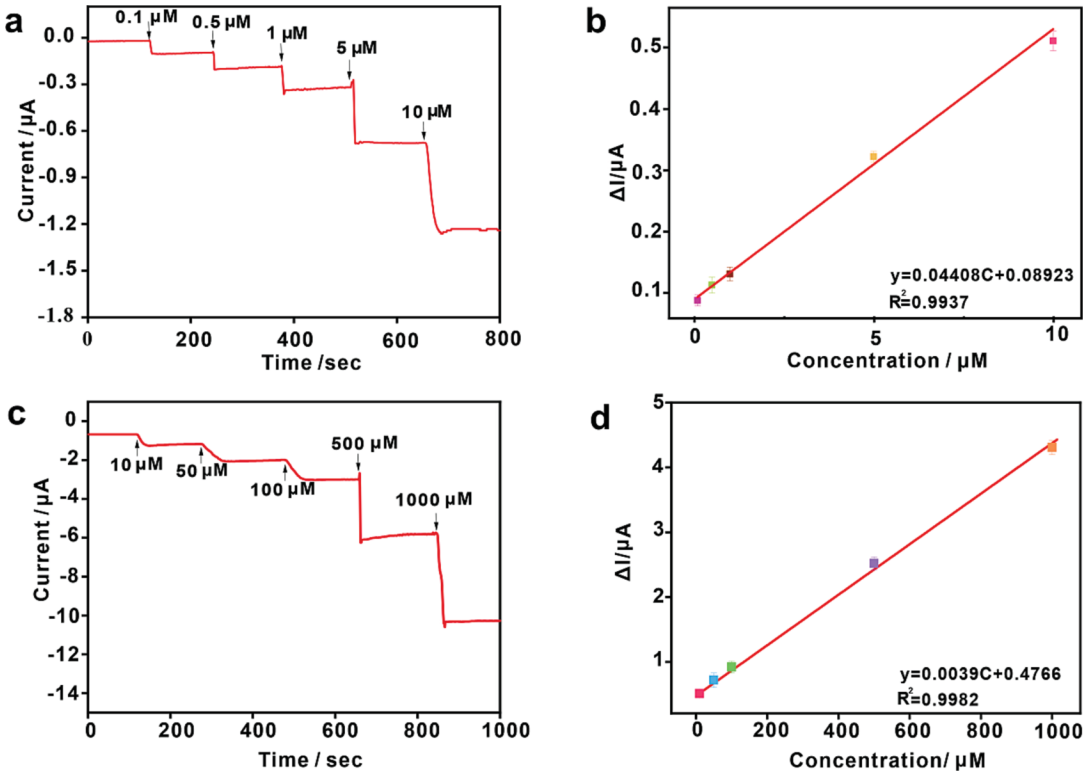

Fig. 4. i-t curves of Ru-NCAG/GCE upon the continuous addition of H_2O_2 to 0.01 M PBS at 0 V. (**a**,**c**) i-t curves with the addition of different concentrations of H_2O_2. (**b**,**d**) Linear correlation between current increment and H_2O_2 concentration.

the sampling interval at 1 s, and the settling time at 2 s. Upon the addition of H_2O_2 at different concentrations into the PBS solution under constant stirring, the amperometric profiles were collected and the measurements were repeated three times at each concentration for evaluating the performance of the Ru-NCAG biosensor for the detection of hydrogen peroxide. Fig. S2 shows the i-t profiles of bare, NCAG, and Ru-NCAG modified GCE in 0.01 M PBS containing 10 μM H_2O_2 at 0 V. One can see that bare and NCAG-modified GCE displayed almost no current response, whereas an obvious and stable current signal appeared with the Ru-NCAG modified GCE, confirming the critical role of Ru species in catalyzing H_2O_2 reduction. It has been known that atomically dispersed ruthenium in carbon aerogels plays a major role in the electrochemical detection of hydrogen peroxide, due to the formation of RuN_x coordination moieties that changed the electron density of the metal center [32]. This significantly enhanced the intrinsic activity of the single-atom site towards the adsorption of hydrogen peroxide. In addition, as most of the Ru single atom sites were on the edge, allowing ready accessibility to hydrogen peroxide. Therefore, large current signals were observed with the Ru-NCAG modified electrodes.

3.3. Detection sensitivity

The sensitivity of Ru-NCAG/GCE for the detection of H_2O_2 was then tested. Upon the addition of H_2O_2 at different concentrations into the PBS buffer solution, the i-t curves were recorded at 0 V. From the i-t profiles in Fig. 4a and 4c, it can be seen that the current increment increased with the increase of H_2O_2 concentration, and the current magnitude showed a good linear relationship with the H_2O_2 concentration in the range of 0.1 ~ 10 μM ($R^2 = 0.9937$) (Fig. 4b) and 10 ~ 1000 μM ($R^2 = 0.9982$) (Fig. 4d). Correspondingly, the limit of detection (LOD) of the electrode was estimated to be 0.01 μM. In comparison with relevant electrochemical sensors in the literature (Table 1), the Ru-NCAG based sensor possessed a lower LOD and a wider linear range.

3.4. Selectivity, stability, and reproducibility

In order to test whether the Ru-NCAG based sensing platform is feasible for practical applications, the performance was evaluated from the perspectives of selectivity, reproducibility and stability. First of all, ascorbic acid (AA), urea, uric acid (UA), glucose, dopamine hydrochloride (DA) were selected as interfering substances, which are common electroactive substances in the human body and are prone to non-specific signals. These interferences were added to the sterile PBS buffer under constant stirring, and the resulting current signals were recorded. From Fig. 5a, it can be observed that when 10 μM H_2O_2 was first added into the buffer solution, a clear current signal was quickly generated; yet the subsequent additions of AA, DA, urea, DA and glucose (at a much higher concentration of 100 μM) did not produce any significant current response. When 10 μM H_2O_2 was then added in the presence of these interferences, the current response increased again accordingly. This shows high selectivity of the Ru-NCAG sensor in H_2O_2 detection (Fig. 5b).

To evaluate the stability of the Ru-NCAG based sensor, the current response to 10 μM H_2O_2 was measured for up to 28 d and repeated three times. As shown in Fig. 5c, the current increment remained virtually unchanged each time the same concentration of H_2O_2 was added at an interval of 7 d. Additionally, five Ru-NCAG modified electrodes were prepared independently and used for the detection of 10 μM H_2O_2 three times. From Fig. 5d, the current responses of each electrode were nearly identical each time, with a low relative standard deviation (RSD) of only 2.43 %. Taken together, these results demonstrate robust stability and reproducibility of the Ru-NCAG based sensor.

Table 1
Comparison of the H_2O_2 detection performance with relevant electrochemical sensors in the literature.

Materials	Detection limit (μM)	Applied potential (V)	Linear range (μM)	Reference
CeO_2/HCCO/MWCNTs/GCE	0.16	−0.25	1 ~ 7310	[40]
Co_3O_4/NPG	0.085	−0.3	2 ~ 2110	[41]
Co-NC/CNF	10	−0.5	10 ~ 5000	[42]
Fe_3C@C/Fe—N—C	0.26	0	1 ~ 6000	[43]
Pt/Fe_3O_4/rGO	1.58	0	100 ~ 2400	[44]
Fe_3O_4/rGO-CNT	0.5	−0.6	1 ~ 2000	[45]
C-ZIF-67/GCE	0.7	−0.35	2.5 ~ 212.5 212.5 ~ 1662.5 1662.5 ~ 6662.5	[46]
Ru-NCAG/GCE	0.01	0	0.1 ~ 1000	This work

3.5. Real-time detection of H_2O_2 release from MCF-7 cells

In order to evaluate the practical applications of the Ru-NCAG based sensor, H_2O_2 released from MCF-7 cells was monitored in real time using Ru-NCAG/GCE at 0 V. As nanomaterials may be cytotoxic [47], the cytotoxicity of Ru-NCAG was first evaluated by the CCK-8 assay. About 2,000 MCF-7 cells in the absence and presence of different concentrations of Ru-NCAG were cultured in a 96-well plate, and the CCK8 reagent was added after 24 h of culture. The optical density (OD) was detected with a microplate reader after 1 h of light protection. As shown in Fig. S3, after co-culturing with the cells at different concentrations of Ru-NCAG (5 ~ 30 μg mL^{-1}) for 24 h, the survival rate of MCF-7 cells remained over 90 %. A normal cell line (mammary epithelial cells) was also used for a comparative assessment and the results are shown in Fig. S4. After co-culturing different concentrations of Ru-NCAG (5 ~ 30 μg mL^{-1}) with MCF-10A cells for 24 h, the cell viability remained above 90 %. This indicates that Ru-NCAG did not impact the metabolic activity of tumor cells, and had minimal effects on normal cells. This suggests good biocompatibility of Ru-NCAG which is promising for the preparation of implantable electrodes for the in vivo detection of hydrogen peroxide.

Subsequently, Ru-NCAG/GCE was used for real-time monitoring of H_2O_2 release from MCF-7 live cells. In practice, 1 mL of a 2×10^6 mL^{-1} cell suspension was transferred into 5 mL of a sterile PBS buffer solution, followed by the addition of fMLP (10 μL, 10 μM), which stimulated the production of H_2O_2 by MCF-7 cells (Fig. 6a). The produced H_2O_2 was released into the solution through the cell membrane and diffuse to the electrode surface, generating an electrochemical signal. As shown in Fig. 6b, no significant current signal was observed when fMLP was added to the PBS solution in the absence of MCF-7 cells (blue curve). In contrast, after MCF-7 cells were added to the solution under the same conditions, a significant current response was detected (purple curve). Then, when fMLP and catalase were added simultaneously to the PBS solution in the presence of MCF-7 cells, no significant current signal could be detected, due to decomposition of H_2O_2 by catalase (orange curve). This proved that the detected current signal was indeed due to H_2O_2 produced by fMLP stimulation of MCF-7 cells. The average current response for the three sets of experiments is shown in Fig. 6c. Based on the amount of current change (approximately 0.2 μA), the total H_2O_2 concentration produced by MCF-7 was estimated to be 2.51 μM (6.275×10^{-15} moL of H_2O_2 produced per cell).

DOX is a common anticancer drug that stimulates the cellular production of H_2O_2, which in excess is cytotoxic to cancer cells and kills them [48]. To evaluate the efficacy of this drug to stimulate H_2O_2 production by MCF-7 cells, 10 μL of DOX was added to a PBS buffer in the absence of MCF-7 cells, and there was no significant change of the current, suggesting that DOX did not produce an interfering signal to affect the subsequent assay. However, when 10 μL DOX was added to PBS containing MCF-7 cells, a significant current response was

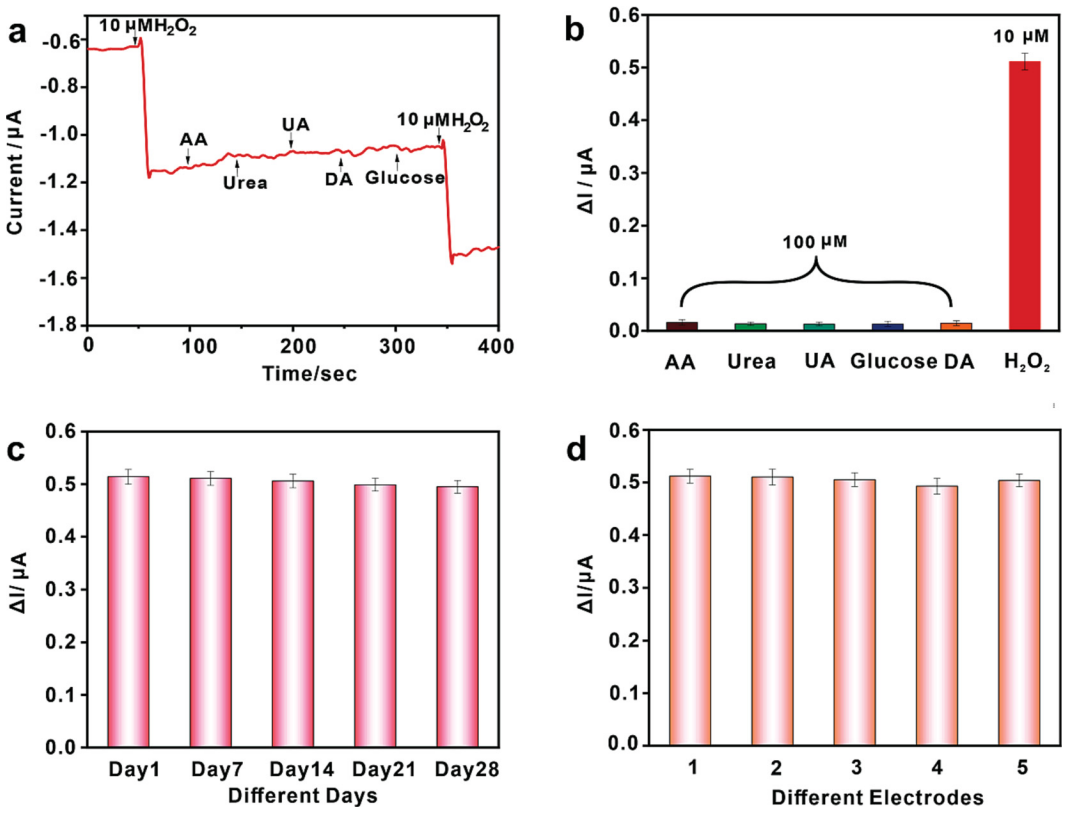

Fig. 5. (a) i-t response of Ru-NCAG upon the additions of H_2O_2 (10 μM) and other interferents of AA (100 μM), Urea (100 μM), UA (100 μM), and DA (100 μM), Glucose (100 μM). (b) Comparison of amperometric response changes for H_2O_2 and other interferents. (c) Stability and (d) reproducibility tests of Ru-NCAG. All tests were carried out in 0.01 M PBS at a constant potential of 0 V.

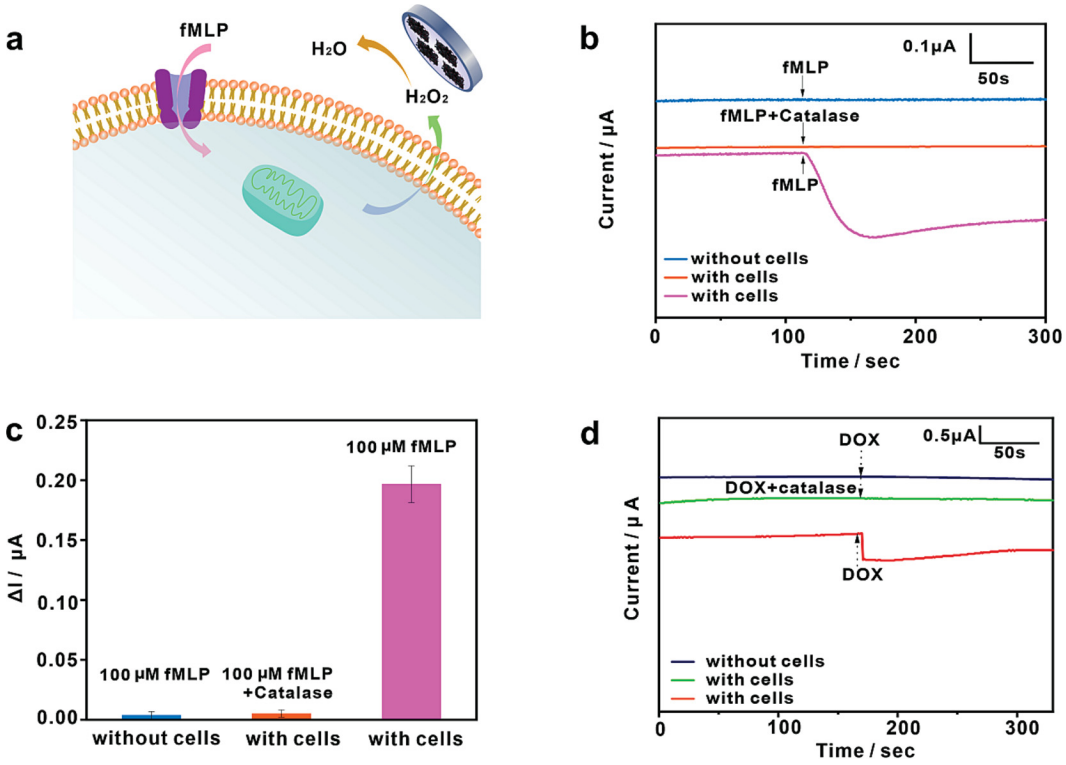

Fig. 6. (a) Schematic of the detection of released H_2O_2 by Ru-NCAG/GCE upon chemical (fMLP) stimulation. (b,d) Amperometric responses of Ru-NCAG/GCE under different additions. (c) Amperometric responses of the different experimental groups.

produced. Upon the addition of catalase, the current signal disappeared, again, due to the decomposition of H_2O_2 by catalase (Fig. 6d). This indicates that the Ru-NCAG based sensor can be used for real-time monitoring of H_2O_2 released from living cells, as well as evaluation of the efficacy of anticancer drugs, which provides a new platform for the screening of clinical anticancer drugs.

4. Conclusion

In summary, ruthenium,nitrogen-codoped carbon aerogels (Ru-NCAG) were prepared by a facile pyrolysis method, and used to modify a glassy carbon electrode for the electrochemical detection of hydrogen peroxide. Ru-NCAG significantly improved interfacial electron transfer and catalyzed H_2O_2 adsorption and reduction. The Ru-NCAG based sensor exhibited excellent H_2O_2 detection at 0 V, with a wide detection range (0.1 μM ~ 1 mM), low detection limit (0.01 μM), and high selectivity even in the presence of common interferences in the cell. Remarkably, the sensor can be used for real-time monitoring of H_2O_2 released from living cells and for the effective screening and evaluation of anticancer drugs, a unique platform for clinical diagnostics.

CRediT authorship contribution statement

Ruiling Qiao: Data curation, Formal analysis, Writing – original draft. **Yongmin Lei:** Data curation, Formal analysis, Writing – original draft. **Qiming Liu:** Conceptualization, Formal analysis. **Lina Tang:** Data curation, Formal analysis. **Xueqian Xiao:** Formal analysis. **Guojun Zhang:** Conceptualization, Formal analysis, Funding acquisition, Writing – original draft. **Ting He:** Formal analysis, Methodology. **Yulin Zhang:** Conceptualization, Formal analysis, Funding acquisition, Writing – original draft. **Chunzi Liang:** Conceptualization, Funding acquisition, Project administration, Resource. **Shaowei Chen:** Conceptualization, Formal analysis, Resources, Writing – review & editing.

Declaration of competing interest

The authors declare that they have no known competing financial interests or personal relationships that could have appeared to influence the work reported in this paper.

Data availability

Data will be made available on request.

Acknowledgments

This work was supported by grants from the Natural Science Foundation of Hubei Province (No. 2023AFD157). C. Z. L. acknowledges support from the 2022 Hubei Provincial Department of Education Young and Middle-Aged Talents Project (No. 20222002). S. W. C. acknowledges partial support from the National Science Foundation (CHE-1900235 and CHE-2003685).

Appendix A. Supplementary data

Supplementary data to this article can be found online at https://doi.org/10.1016/j.jelechem.2023.117997.

References

[1] H. Sies, D.P. Jones, Reactive oxygen species (ROS) as pleiotropic physiological signalling agents, Nat. Rev. Mol. Cell Biol. 21 (2020) 363–383, https://doi.org/10.1038/s41580-020-0230-3.
[2] M.T. Lin, M.F. Beal, Mitochondrial dysfunction and oxidative stress in neurodegenerative diseases, Nature 443 (2006) 787–795, https://doi.org/10.1038/nature05292.
[3] M.S. Shim, Y. Xia, A Reactive Oxygen Species (ROS)-Responsive Polymer for Safe, Efficient, and Targeted Gene Delivery in Cancer Cells, Angew. Chem. Int. Edit. 52 (2013) 6926–6929, https://doi.org/10.1002/anie.201209633.
[4] C.X. Guo, F.P. Hu, C.M. Li, P.K. Shen, Direct electrochemistry of hemoglobin on carbonized titania nanotubes and its application in a sensitive reagentless hydrogen peroxide biosensor, Biosens. Bioelectron. 24 (2008) 825–830, https://doi.org/10.1016/j.bios.2008.07.007.
[5] H. Sies, Role of metabolic H_2O_2 generation: redox signaling and oxidative stress, J. Biol. Chem. 289 (2014) 8735–8741, https://doi.org/10.1074/jbc.R113.544635.
[6] C.C. Winterbourn, Biological Production, Detection, and Fate of Hydrogen Peroxide, Antioxid. Redix. Signal. 29 (2018) 541–551, https://doi.org/10.1089/ars.2017.7425.
[7] G. Minotti, P. Menna, E. Salvatorelli, G. Cairo, L. Gianni, Anthracyclines: molecular advances and pharmacologic developments in antitumor activity and cardiotoxicity, Pharmacol. Rev. 56 (2004) 185–229, https://doi.org/10.1124/pr.56.2.6.
[8] V. Patel, P. Kruse, P.R. Selvaganapathy, Solid State Sensors for Hydrogen Peroxide Detection, Biosensors-Basel 11 (2020) 9, https://doi.org/10.3390/bios11010009.
[9] C.S. Pundir, R. Deswal, V. Narwal, Quantitative analysis of hydrogen peroxide with special emphasis on biosensors, Bioprocess Biosyst. Eng. 41 (2018) 313–329, https://doi.org/10.1007/s00449-017-1878-8.
[10] M. Peng, Y. Zhao, D. Chen, Y. Tan, Free-standing 3D electrodes for electrochemical detection of hydrogen peroxide, ChemCatChem 11 (2019) 4222–4237, https://doi.org/10.1002/cctc.201900913.
[11] Y. Yu, M. Pan, J. Peng, D. Hu, Y. Hao, Z. Qian, A review on recent advances in hydrogen peroxide electrochemical sensors for applications in cell detection, Chin. Chem. Lett. 33 (2022) 4133–4145, https://doi.org/10.1016/j.cclet.2022.02.045.
[12] S. Wang, Y. Liu, A. Zhu, Y. Tian, In Vivo Electrochemical Biosensors: Recent Advances in Molecular Design, Electrode Materials, and Electrochemical Devices, Anal. Chem. 95 (2023) 388–406, https://doi.org/10.1021/acs.analchem.2c04541.
[13] S. Singh, M. Singh, K. Mitra, R. Singh, S.K. Sen Gupta, I. Tiwari, B. Ray, Electrochemical sensing of hydrogen peroxide using brominated graphene as mimetic catalase, Electrochim. Acta 258 (2017) 1435–1444, https://doi.org/10.1016/j.electacta.2017.12.006.
[14] K. Atacan, M. Ozacar, Construction of a non-enzymatic electrochemical sensor based on CuO/g-C_3N_4 composite for selective detection of hydrogen peroxide, Mater. Chem. Phys. 266 (2021) 124527, https://doi.org/10.1016/j.matchemphys.2021.124527.
[15] L. Li, Y. Hu, D. Deng, H. Song, Y. Lv, Highly sensitive cataluminescence gas sensors for 2-butanone based on g-C_3N_4 sheets decorated with CuO nanoparticles, Anal. Bioanal. Chem. 408 (2016) 8831–8841, https://doi.org/10.1007/s00216-016-9906-0.
[16] X. Gao, W. Ma, J. Mao, C. He, W. Ji, Z. Chen, W. Chen, W. Wu, P. Yu, L. Mao, A single-atom Cu–N_2 catalyst eliminates oxygen interference for electrochemical sensing of hydrogen peroxide in a living animal brain, Chem. Sci. 12 (2021) 15045–15053, https://doi.org/10.1039/D1SC04755H.
[17] X. Zhao, Y. Liu, Origin of selective production of hydrogen peroxide by electrochemical oxygen reduction, J. Am. Chem. Soc. 143 (2021) 9423–9428, https://doi.org/10.1021/jacs.1c02186.
[18] K. Jiang, S. Back, A.J. Akey, C. Xia, Y. Hu, W. Liang, D. Schaak, E. Stavitski, J. K. Nørskov, S. Siahrostami, H. Wang, Highly selective oxygen reduction to hydrogen peroxide on transition metal single atom coordination, Nat. Commun. 10 (2019) 3997, https://doi.org/10.1038/s41467-019-11992-2.
[19] H. Hu, F. Wang, X. Ding, S. Imhanria, W. Wang, J. Zhang, Green fabrication of Pt nanoparticles via tea-polyphenols for hydrogen peroxide detection, Colloids Surf. A, Physicochem. Eng. Asp. 637 (2022) 128201, https://doi.org/10.1016/j.colsurfa.2021.128201.
[20] R.C. Peña, V.O. Silva, F.H. Quina, M. Bertotti, Hydrogen peroxide monitoring in Fenton reaction by using a ruthenium oxide hexacyanoferrate/multiwalled carbon nanotubes modified electrode, J. Electroanal. Chem. 686 (2012) 1–6, https://doi.org/10.1016/j.jelechem.2012.08.037.
[21] K. Wang, Y. Du, Y. Li, X. Wu, H. Hu, G. Wang, Y. Xiao, S. Chou, G. Zhang, Atomic-level insight of sulfidation-engineered Aurivillius-related $Bi_2O_2SiO_3$ nanosheets enabling visible light low-concentration CO_2 conversion, Carbon Energy 5 (2023) e264, https://doi.org/10.1002/cey2.264.
[22] Y.L. Wang, S. Gurses, N. Felvey, A. Boubnov, S.S. Mao, C.X. Kronawitter, In Situ Deposition of Pd during Oxygen Reduction Yields Highly Selective and Active Electrocatalysts for Direct H_2O_2 Production, ACS Catal. 9 (2019) 8453–8463, https://doi.org/10.1021/acscatal.9b01758.
[23] X.L. Tian, Y.Y. Xu, W. Zhang, T. Wu, B.Y. Xia, X. Wang, Unsupported Platinum-Based Electrocatalysts for Oxygen Reduction Reaction, ACS Energy Lett. 2 (2017) 2035–2043, https://doi.org/10.1021/acsenergylett.7b00593.
[24] X. Xie, D.P. Wang, C. Guo, Y. Liu, Q. Rao, F. Lou, Q. Li, Y. Dong, Q. Li, H.B. Yang, F. X. Hu, Single-Atom Ruthenium Biomimetic Enzyme for Simultaneous Electrochemical Detection of Dopamine and Uric Acid, Anal. Chem. 93 (2021) 8, https://doi.org/10.1021/acs.analchem.0c05191.
[25] Y. Peng, B. Lu, S. Chen, Carbon-Supported Single Atom Catalysts for Electrochemical Energy Conversion and Storage, Adv. Mater. 30 (2018) e1801995.
[26] B. Lu, Q. Liu, S. Chen, Electrocatalysis of Single-Atom Sites: Impacts of Atomic Coordination, ACS Catal. 10 (2020) 7584–7618, https://doi.org/10.1021/acscatal.0c01950.
[27] Y. Wang, H. Su, Y. He, L. Li, S. Zhu, H. Shen, P. Xie, X. Fu, G. Zhou, C. Feng, D. Zhao, F. Xiao, X. Zhu, Y. Zeng, M. Shao, S. Chen, G. Wu, J. Zeng, C. Wang, Advanced Electrocatalysts with Single-Metal-Atom Active Sites, Chem. Rev. 120 (2020) 12217–12314, https://doi.org/10.1021/acs.chemrev.0c00594.

[28] Y. Chen, S. Hu, F. Nichols, F. Bridges, S. Kan, T. He, Y. Zhang, S. Chen, Carbon aerogels with atomic dispersion of binary iron-cobalt sites as effective oxygen catalysts for flexible zinc-air batteries, J. Mater. Chem. A 8 (2020) 11649–11655, https://doi.org/10.1039/d0ta04633g.

[29] T. He, B. Lu, Y. Chen, Y. Wang, Y. Zhang, J.L. Davenport, A.P. Chen, C. Pao, M. Liu, Z. Sun, A. Stram, A. Mordaunt, J.J. Velasco, Y. Ping, Y. Zhang, S. Chen, Nanowrinkled Carbon Aerogels Embedded with FeNx Sites as Effective Oxygen Electrodes for Rechargeable Zinc-Air Battery, Research 2019 (2019) 6813585, https://doi.org/10.34133/2019/6813585.

[30] B. Zhu, C. Qu, S. Gao, Z. Liang, H. Zhang, R. Zou, Ultralow Loading Ruthenium Nanoparticles on Nitrogen-Doped Graphene Aerogel for Trifunctional Electrocatalysis, ChemCatChem. 10 (2018) 1113–1121, https://doi.org/10.1002/cctc.201701691.

[31] Y. Song, T. He, Y. Zhang, C. Yin, Y. Chen, Q. Liu, Y. Zhang, S. Chen, Cobalt single atom sites in carbon aerogels for ultrasensitive enzyme-free electrochemical detection of glucose, J. Electroanal. Chem. 906 (2022), 116024, https://doi.org/10.1016/j.jelechem.2022.116024.

[32] T. He, Y.Y. Song, Y. Chen, X.W. Song, B.Z. Lu, Q.M. Liu, H.T. Liu, Y. Zhang, X. P. Ouyang, S.W. Chen, Atomically dispersed ruthenium in carbon aerogels as effective catalysts for pH-universal hydrogen evolution reaction, Chem. Eng. J. 442 (2022) 136337, https://doi.org/10.1016/j.cej.2022.136337.

[33] T. He, Y. Chen, Q. Liu, B. Lu, X. Song, H. Liu, M. Liu, Y.N. Liu, Y. Zhang, X. Ouyang, S. Chen, Theory-Guided Regulation of FeN4 Spin State by Neighboring Cu Atoms for Enhanced Oxygen Reduction Electrocatalysis in Flexible Metal-Air Batteries, Angew. Chem. Int. Edit. 61 (2022) e202201007.

[34] Y. Chen, T. He, Q. Liu, Y. Hu, H. Gu, L. Deng, H. Liu, Y. Liu, Y. Liu, Y. Zhang, S. Chen, X. Ouyang, Highly durable iron single-atom catalysts for low-temperature zinc-air batteries by electronic regulation of adjacent iron nanoclusters, Appl. Catal. B: Environ. 323 (2023), 122163, https://doi.org/10.1016/j.apcatb.2022.122163.

[35] L. Xiao, K. Li, B. Liu, J. Tu, T. Li, Y. Li, G. Zhang, A pH-sensitive field-effect transistor for monitoring of cancer cell external acid environment, Talanta. 252 (2023), 123764, https://doi.org/10.1016/j.talanta.2022.123764.

[36] B. Lu, L. Guo, F. Wu, Y. Peng, J.E. Lu, T.J. Smart, N. Wang, Y.Z. Finfrock, D. Morris, P. Zhang, N. Li, P. Gao, Y. Ping, S. Chen, Ruthenium atomically dispersed in carbon outperforms platinum toward hydrogen evolution in alkaline media, Nat. Commun. 10 (2019) 631, https://doi.org/10.1038/s41467-019-08419-3.

[37] Q. Liu, B. Lu, F. Nichols, J. Ko, R. Mercado, F. Bridges, S. Chen, Rapid preparation of carbon-supported ruthenium nanoparticles by magnetic induction heating for efficient hydrogen evolution reaction in both acidic and alkaline media, SusMat. 2 (2022) 335–346, https://doi.org/10.1002/sus2.66.

[38] S. Feng, M. Ming, M. Wang, X. Wang, D. He, P. Jiang, Y. Chen, Uniformly distributed ruthenium nanocrystals as highly efficient peroxidase for hydrogen peroxide colorimetric detection and nitroreductase for 4-nitroaniline reduction, Chem. Commun. 56 (2020) 11235–12347, https://doi.org/10.1039/d0cc04101g.

[39] F.J. Kristine, C.R. Johnson, S. O'Donnell, R.E. Shepherd, Reduction of hydrogen peroxide by ruthenium(II) ammine complexes: the surprisingly identical mechanism for hexaammineruthenium(2+), pentaammine(aquo)ruthenium(2+), and pentaammine(1-methylimidazole)ruthenium(2+), Inorg. Chem. 19 (1980) 2280–2284, https://doi.org/10.1021/ic50210a018.

[40] J. Xie, D. Cheng, Z. Zhou, X. Pang, M. Liu, P. Yin, Y. Zhang, H. Li, X. Liu, S. Yao, Hydrogen peroxide sensing in body fluids and tumor cells via insitu produced redox couples on two-dimensional holey $CuCo_2O_4$ nanosheets, Microchim. Acta. 187 (2020) 10, https://doi.org/10.1007/s00604-020-04389-2.

[41] Y. Pei, M. Hu, X. Tang, W. Huang, Z. Li, S. Chen, Y. Xia, Ultrafast one-pot anodic preparation of Co_3O_4/nanoporous gold composite electrode as an efficient nonenzymatic amperometric sensor for glucose and hydrogen peroxide, Anal. Chim. Acta. 1059 (2019) 10, https://doi.org/10.1016/j.aca.2019.01.059.

[42] M.A. Riaz, Z. Yuan, A. Mahmood, F. Liu, X. Sui, J. Chen, Q. Huang, X. Liao, L. Wei, Y. Chen, Hierarchically porous carbon nanofibers embedded with cobalt nanoparticles for efficient H_2O_2 detection on multiple sensor platforms, Sens. Actuat. B: Chem. 319 (2020), 128243, https://doi.org/10.1016/j.snb.2020.128243.

[43] X. Wei, S. Song, W. Song, W. Xu, L. Jiao, X. Luo, N. Wu, H. Yan, X. Wang, W. Gu, L. Zheng, C. Zhu, Fe_3C-Assisted Single Atomic Fe Sites for Sensitive Electrochemical Biosensing, Anal. Chem. 93 (2021) 5334–5342, https://doi.org/10.1021/acs.analchem.1c00635.

[44] X. Zhao, Z. Li, C. Chen, Y. Wu, Z. Zhu, H. Zhao, M. Lan, A Novel Biomimetic Hydrogen Peroxide Biosensor Based on Pt Flowers-decorated Fe_3O_4/Graphene Nanocomposite, Electroanalysis. 29 (2017) 6, https://doi.org/10.1002/elan.201600793.

[45] O. Garate, L.S. Veiga, P. Tancredi, A.V. Medrano, L.N. Monsalve, G. Ybarra, High-performance non-enzymatic hydrogen peroxide electrochemical sensor prepared with a magnetite-loaded carbon nanotube water borne ink, J. Electroanal. Chem. 915 (2022) 116372, https://doi.org/10.1016/j.jelechem.2022.116372.

[46] Y. Dong, J. Zheng, Environmentally friendly synthesis of Co-based zeolitic imidazolate framework and its application as H_2O_2 sensor, Chem. Eng. J. 392 (2020), 123690, https://doi.org/10.1016/j.cej.2019.123690.

[47] Y. Zhang, S.F. Ali, E. Dervishi, Y. Xu, Z. Li, D. Casciano, A.S. Biris, Cytotoxicity Effects of Graphene and Single-Wall Carbon Nanotubes in Neural Phaeochromocytoma-Derived PC12 Cells, ACS Nano. 4 (2010) 3181–3186, https://doi.org/10.1021/nn1007176.

[48] R.K. Kankala, P. Tsai, Y. Kuthati, P. Wei, C. Liu, C. Lee, Overcoming multidrug resistance through co-delivery of ROS-generating nano-machinery in cancer therapeutics, J. Mater. Chem. B 5 (2017) 1507–1517, https://doi.org/10.1039/C6TB03146C.